# Graph Theoretical Network Analysis and Pharmacoinformatics-Based Investigation of Bioactive Compounds of *Rasam* (South Indian Recipe) Against Human Cancer

**Arjun Kumar Kalimuthu**
Kalasalingam Academy of Research and Education
**Theivendran Panneerselvam**
Swamy Vivekanadha College of Pharmacy
**Pavadai Parasuraman**
M.S. Ramaiah University of Applied Sciences, M S R Nagar
**Sureshbabu Ram Kumar Pandian**
Kalasalingam Academy of Research and Education
**Sankaranarayanan Murugesan**
Birla Institute of Technology & Science Pilani
**Damodar Nayak Ammunje**
M.S. Ramaiah University of Applied Sciences, M S R Nagar
**Sattanathan Kumar**
Paavai College of Pharmacy and Research
**Sankarganesh Arunachalam**
Kalasalingam Academy of Research and Education
**Selvaraj Kunjiappan** ( selvaraj.k@klu.ac.in )
Kalasalingam Academy of Research and Education

**Research Article**

**Keywords:** Rasam, graph theoretical network analysis, in silico modelling, mitogen-activated protein kinase, ADMET, molecular dynamics.

**Posted Date:** June 30th, 2021

**DOI:** https://doi.org/10.21203/rs.3.rs-663436/v1

## Abstract

Spice-rich recipes are referred to as "functional foods" because they include a variety of bioactive chemicals that have health-promoting properties in addition to their nutritional value. Using pharmacoinformatics-based analysis, we explored the relevance of bioactive chemicals found in *rasam* (a south Indian cuisine) against oxidative stress-induced human malignancies. The *rasam* is composed of twelve main ingredients, each of which contains a variety of bioactive chemicals. Sixty-six bioactive compounds were found from these ingredients, and their structures were downloaded from Pubchem. To find the right target via graph theoretical analysis (mitogen-activated protein kinase (MAPK)) and display their signaling route, a network was built. Among the identified compounds sixty-six bioactive compounds were used for *in silico* molecular docking study against MAPK, the top four compounds were chosen for further study based on their docking score and binding affinities. *In silico* predicted ADMET characteristics of the titled compounds were used to assess their drug-likeness. Molecular dynamics (MD) simulation modelling methodology were also used to analyze the effectiveness and safety profile of top four selected bioactive chemicals based on the docking score, as well as to assess the stability of the MAPK-ligand complex structure. Surprisingly, the discovered docking scores against MAPK revealed that the titled bioactive chemicals distribution varied between -3.5 and -10.6 kcal/mol. MD simulation validated the stability of four chemicals at the MAPK binding pockets, including Assafoetidinol A (ASA), Naringin (NAR), Rutin (RUT), and Tomatine (TOM). According to the results obtained, fifty of the sixty-six compounds showed higher binding affinity (-6.1 to -10.6 kcal/mol), and four of these compounds may be used as lead compounds to protect cells against oxidative stress-induced human malignancies.


## Introduction

Cancer is defined as unregulated cell or tissue growth that may spread to other parts of the bodys. It is the second greatest cause of mortality in the world, behind cardiovascular illnesses, and the number of cases continues to rise[1]. According to the GLOBOCON-2020 report, there is around 19.30 million new cancer cases diagnosed and 10.00 million cancer deaths worldwide[2]. A range of modifiable health behaviours, such as high fat and simple carbohydrate diet, bad eating habits as well as poor physical activity contributes to the sudden rise in cancer incidences[3]. Several studies have shown that dysregulated nutrition and sedentary life style are key factors in the cellular redox process, resulting in unwanted by-products such as reactive oxygen species (ROS), reactive nitrogen species (RNS), and DNA reactive aldehyde[4–6]. In mitochondria, ROS is an unavoidable by-product of oxidative phosphorylation[7]. ROS is a two-edged sword that has both helpful (at low concentration) and harmful (at high concentration) properties. At low concentration, ROS regulates cellular activities such as cell cycle, proliferation, differentiation, migration, and death while an increased quantity of ROS may damage proteins, nucleic acids, lipids, membranes, and organelles, it also reduces cell viability and causes apoptosis[8,9].

The production of reactive oxygen species (ROS) in cells is inhibited by a number of antioxidant defense mechanisms. Antioxidant stress response genes serves as an important function of protecting cells and tissues from toxins and oxidative stress[10]. Oxidative stress sensitive genes accomplish ROS scavenging by secreting antioxidant enzymes including superoxide dismutase (SOD), catalase, glutathione peroxidase, peroxiredoxins, and other non-enzymatic compounds such as flavonoids, carotenoids, glutathione, α-lipoic acid, iron chelators, vitamins A, C and E[11]. Furthermore, increased levels of intracellular ROS beyond a certain threshold cause down regulation of cellular antioxidant pathways and enzyme systems, resulting in malignant transformation via various molecular targets such as nuclear factor-B (NF-B), nuclear factor E2 (erythroid-derived 2)-related factor 2 (Nrf2), Kelch like-ECH-associated protein 1 (Keap1), mitogen-activated protein kinase (MAPK) and phosphoinositide 3-kinase (PI3K)[12].

Spices are used in cuisine all around the globe for their taste, flavour and their health advantages[13]. Because, they contain numerous bioactive components, certain spices have been utilized in Indian traditional medicine to prevent and cure numerous ailments, including cancer[14]. Capsaicin (red pepper)[1], curcumin (turmeric)[15], piperine (black pepper)[16], lycopene (tomato)[17], myricetin (tea)[18], and rutin (buckwheat)[19] are a few examples of bioactive chemicals that have been shown to possess antioxidant and anticancer properties. "*Rasam*" is a famous South Indian spicy soup that has been made fresh every day and served with rice[20]. Tamarind, red pepper, black pepper, cumin seed, fenugreek, asafoetida, garlic, tomato, coriander, curry leaves, sesame oil, and mustard are the main flavors (spices) of *rasam*[21]. These spices used to make *rasam*, a "functional food" include a plethora of bioactive chemicals that have been linked to improved tumor prognosis[22]. The synergistic activity of a mixed bioactive chemicals is always greater than that of a single component[23]. Furthermore, these bioactive chemicals function via many signaling pathways and display anticancer activity by blocking certain signaling cascades that drive unregulated cell division and proliferation[24]. Bioactive substances may also inhibit the malignant transformation by targeting pro-tumorigenic cells or the pro-metabolic carcinogen's conversion[25].

By affecting numerous genes and transcription factors, cancer cells have acquired resistance to cancer treatments. These genes and transcription factors are thought to be an important targets for slowing the development of cancer[26]. The signaling networks, such as genes, proteins, and enzymes, are shown in this perspective using graph theoretical network analysis. The selection of good target signaling network

may be aided by graph theoretical network analysis [27]. It also gives data on the active site and molecular interactions of bioactive substances, which may help in the *in silico* molecular docking study. As a result, the current research used pharmacoinformatics to examine the relevance of bioactive chemicals found in *rasam* spices against oxidative stress-induced human malignancies. The predicted ADMET (absorption, distribution, metabolism, excretion, and toxicity) characteristics of the bioactive compounds were also investigated. Further, molecular dynamics simulation was investigated to determine the stability and binding modes of selected bioactive compounds with an appropriate cancer receptor protein.

# Materials And Methods

### Graph theoretical network analysis

The graph theoretical network analysis was carried out using Cytoscape software 3.7.1 and the Kyoto Encyclopedia of Genes and Genomes (KEGG) database[28]. The functions of numerous genes and proteins involved in the MAPK (ko04010) signaling pathways were given in the current research work (Fig. 1). Based on centrality criteria such as degree, proximity, eccentricity, eigen vector, and radiality, the network has 129 nodes and 177 edges. The measured values of degree (16), closeness (15.49), eccentricity (1), eigen vector (0.3564), radiality (9.18), and stress (1256) have shown the threshold value of all measures as well as significant node in the network. (Tables 1 and 2).

### Protein preparation

The RCSB Protein Data Bank (PDB http://www.rcsb.org/pdb) provided the X-ray crystallographic structure of MAPK (PDB ID: 7AQB)[29]. Prior to analysis, the protein was cleaned and missing residues were inserted using Swiss-PDB Viewer v4.1.0's prepare protein process. The file was named target.pdb and saved for further analysis. We also utilized BIOVIA Discovery Studio Visualizer 4.0 software (Accelrys Software Inc., San Diego, CA) in order to determine the protein structure and amino acid position from active regions, which was then utilized for molecular docking study.

### Active compounds retrieval and preparation

We found that around sixty-six bioactive components from twelve spices were used to make *rasam*. The identified 66 components were collected using the data repository (Indian Medicinal Plants, Phytochemistry, and Therapeutics (IMPPAT)), previously published studies [30] and public database PubChem (http://pubch em.ncbi.nlm.nih.gov).

### Binding site identification

A binding site in the target is a particular location on an enzyme / protein that permits the enzyme to attach to certain molecules and perform a chemical reaction. The major strategy to treat a disease is the binding of ligands or bioactive chemicals to the specific location of a protein / enzyme. This helps the bioactive chemicals to create enough contact sites in order to establish robust interaction with target enzymes by ensuring optimal and favourable catalytic areas. Using the Prank Web (https://prankweb.cz/) server, all possible active binding sites of targeted compounds were found for further analysis. Using the PyRx program, a receptor grid was created once the active site of protein was selected.

### Molecular docking

Molecular docking approach is a crucial component of structural biology research, and it is one among the widely used technique in the process of drug design. The PyRx tool[31] and AutoDock Vina program[32] was used to accomplish the molecular docking study. The ligand was selected bioactive chemicals, and the receptor was MAPK (PDB ID: 7AQB). Polar hydrogen atoms and Kollman partial charges were introduced into the 3D structure using PyRx software. To compute docking energy affinities (kcal / mol), the receptor and ligand files were stored in .pdbqt format. For each ligand, AutoDock Vina calculated the energy affinity values of up to ten different docking positions. AutoDock Vina effects were used to calculate each complex affinity energies based on the ligand conformation at the active binding site with RMSD between the original and subsequent structures taken into consideration. The amount of hydrogen bonds and non-covalent interactions for each complex were calculated using Discovery Studio Visualizer, which produced details, compounds, and interaction pictures (2D and 3D)[33].

### *In silico* pharmacokinetic properties prediction

*In silico* prediction of pharmacokinetic (ADME) properties of the selected bioactive chemicals plays a major role in determining its integrity and efficiency. Selected bioactive chemicals into account, properties like bioavailability, brain penetration, oral absorption, carcinogenicity, and other human intestinal absorption properties of the active bio-compounds have been determined using SwissADME (www.swissadme.ch) webserver. The SwissADME webserver is a free tool that can predict the pharmacokinetic and drug-likeness properties of the test bioactive compounds[34].

### Toxicity prediction

Toxicity was predicted by determining the safety profile of the intended bioactive chemicals, which must have deadly effects on people and cause organ damage. As a result, the toxicity of the chosen bioactive chemicals was assessed using ProTox-II web-based server (http://tox.charite.de/protox II)[35].

### Molecular dynamics stimulation

The molecular dynamic simulation was evaluated to determine the binding stability, confirmation and interaction modes between the selected bioactive compounds (ligands) and receptor (MAPK). The selected ligand-MAPK complex files were subjected to molecular dynamics studies using GROMACS 2019.2 software[36]. The selected ligands topology was downloaded from PRODRG server[37]. The system preparation of all the complexes were as described earlier[19]. For molecular dynamic simulation, first vacuum was minimized using the steepest descent algorithm for 5000 steps. The complex structure was solvated in a cubic periodic box of 0.5 nm with a simple point charge (SPC) water model. The complex system was subsequently maintained with an appropriate salt concentration of 0.15M by adding a suitable amount of Na+ and Cl− counter ions. Each complex was allowed a simulation time of 50 ns from the NPT (Isothermal-Isobaric, constant number of particles, pressure, and temperature) equilibration was subjected in NPT ensemble for final run. The trajectory analysis of root means square deviation (RMSD) and root mean square fluctuation (RMSF) was performed in the GROMACS simulation package through the online server “WebGRO for Macromolecular Simulations (https://simlab.uams.edu/)”.

## Results

### Bioactive compounds retrieval and preparation

The accessible bioactive components of the requested spices (tamarind, red pepper, black pepper, cumin seed, fenugreek, asafoetida, garlic, tomato, coriander, curry leaves, sesame oil, and mustard) were searched using IMPART database. From the database, a list of sixty-six important bioactive compounds were selected from the desired twelve spices depicted in Table 3.

### Binding site identification

The crystal structure of MAPK (PDB: 7AQB) included 11 binding sites, according to binding site analyses. The protein's recovered binding site residue was shown in Figure 2. Molecular docking investigations were also conducted using the obtained complex structure of the binding sites. Grid generation in molecular docking research results in more reliable ligand posture scoring. As a result, we created a receptor grid for the selected MAPK protein based on the previously acquired binding site residues to achieve more precise scoring of our ligand poses. A receptor grid with a box diameter of X = 38.6666, Y = 62.5914, and Z = 31.9740 in angstrom (Å) was created and utilized further for molecular docking experiments.

### Molecular docking

The optimum intermolecular interaction between the target protein and bioactive chemicals were investigated using molecular docking analysis. To analyze their binding capability, a specific number of bioactive chemicals (sixty-six) were docked against MAPK using PyRx tools AutoDock Vina. Twelve bioactive chemicals were shown to have a higher binding affinity (>-9 kcal/mol) with the target protein. The binding affinity of the bioactive compounds following molecular docking was found to be scattered, ranging from -3.50 to -10.60 kcal/mol, as illustrated in Fig. 3 and Table 3. The top four compounds (Assafoetidinol A (-9.80 kcal/mol), Naringin (-9.60 kcal/mol), Rutin (-9.80 kcal/mol), and Tomatine (-10.60 kcal/mol)) were chosen for future research based on their affinities with the active site aminoacid residues.

### Interpretation of protein–ligand interactions

The interactions formed between the selected four ligands and MAPK has been visualized using BIOVIA Discovery studio visualizer tool. It was observed that compound CID: 2041593 (Assafoetidinol A) showed better interaction with binding affinity (-9.80 kcal/mol). Compound CID: 12041593 (Assafoetidinol A) formed four van der walls interactions with TYR (3.81 Å), GLU (3.57 Å), GLU (3.74 Å) and TRP (3.86 Å), two conventional and two carbon hydrogen bonds TYR (2.09 Å), ALA (2.10 Å) and GLU (3.58 Å), ASN (2.85 Å) respectively. Alkyl and Pi-Alkyl bond was also found at the position ARG (3.64 Å), ALA (3.75 Å), and PRO547 (3.67 Å), respectively showed in Figure 4 and Table 4. For the compound CID: 442428 (Naringin) it has been observed four hydrophobic and four hydrogen bonds with desired active site aminoacid residues of MAPK. Hydrophobic interactions with ALA (3.84 Å), LYS (3.76 Å), GLU (3.86 Å) and THR (3.75 Å), and four hydrogen bonds GLU (3.22 Å), LYS (3.11 Å), ASN (3.99 Å) and GLY (3.04 Å), respectively showed in Figure 5 and Table 4. In the case of CID: 5280805 Rutin exhibited four hydrophobic bonds with ARG (3.64 Å), GLU (3.59 Å), THR (3.71 Å) TRP (3.71 Å) and six hydrogen bonding with ARG (3.84 Å), ALA (4.03 Å), GLU (3.10 Å), ASN (3.20 Å), TYR (2.93 Å), GLU (3.44 Å) between active site aminoacid residues of desired protein MAPK, depicted in Figure 6 and Table 4. For, CID: 28523 (Tomatine), it has observed two hydrophobic bonding with TYR (3.97 Å), VAL (3.75 Å), and four hydrogen bonding with GLY (3.42 Å), ARG (3.25 Å), ASN (4.08 Å), THR (3.25 Å) between the target protein, and showed in Figure 7 and Table 4.

### *In silico* Absorption, Distribution, Metabolism, and Excretion (ADME) prediction analysis

Absorption, Distribution, Metabolism, and Excretion (ADME) properties was assessed through SwissADME (www.swissadme.ch) webserver, which demonstrated that key bioactive compounds from *rasam*, i.e. Assafoetidinol A possessed better human intestinal absorption property. Naringin, Rutin and Tomatine have moderate absorption properties. In general, moderate intestinal absorption leads to the bioactive compounds of food (*rasam*) might be better consumed from the gastrointestinal tract upon oral administration. The higher number of H-bonds are possibly measured to be involved during protein ligand binding. From the result, the drug-likeness properties of four compounds showed better results (+0.55 Assafoetidinol A, and +0.17 for other three compounds) thereby relating with molecular properties, these four compounds were predicted to have better chances as a possible drug-relevant candidate with anticancer potential. The ADME properties like lipophilicity (dissolve in fats, oils and nonpolar solvents), water solubility and drug-likeness of the selected compounds have been investigated and presented in Table 5.

### Analysis of toxicity

*In silico* toxicity prediction of the selected four compounds has been performed using ProTox-II web-based server. The server has identified drug-induced hERG toxicity, AMES toxicity, $LD_{50}$, hepatotoxicity, skin sensitization, *Tetrahymena pyriformis* (TP) toxicity, and minnow toxicity which was listed in Table 6.

### Molecular dynamics simulation

Although, protein–ligand docking was widespread and has successful use, it just gives the static view of the binding pose of ligand in active site of the receptor similar to photo image. Molecular dynamics (MD) must be employed to simulate the dynamics of atoms in the system as a function of time with integration of Newton's equations of motions [38]. MD simulations for 50 ns were carried out for the top four complexes obtained from the docking studies, that is 7AQB-ASA, 7AQB-NAR, 7AQB-RUT, 7AQB-TOM and unbounded apo form of the target MAPK protein (PDB ID: 7AQB) and their results were interpreted. To decipher the stability and fluctuations of these complexes, MD trajectories analysis was performed with the help of RMSD (Root Mean Square Deviation), RMSF (Root Mean Square Fluctuation), RG (Radius of gyration) and SASA (Solvent Accessible Surface Area) of receptor atoms.

RMSD is an important parameter to analyse the equilibration of MD trajectories and check the stability of complex systems during the simulation process. RMSD of the protein backbone atoms were plotted against time to assess its variations in structural confirmation. Initially, the 7AQB-ASA complex showed variations in backbone RMSD till 30 ns ranging from 0.15 to 0.44 nm. The stable conformation was attained in the time period between 21-50 ns with no considerable deviations in the values (Figure 8). 7AQB-NAR complex showed variations in backbone RMSD till 20 ns ranging from 0.17 to 0.43 nm. The stable conformation was attained in the time period between 21-50 ns with no considerable deviations in the values (Figure 8). The 7AQB-RUT complex showed variations in backbone RMSD till 30 ns ranging from 0.13 to 0.35 nm. The stable conformation was attained in the time period between 31-50 ns with no considerable deviations in the values (Figure 8). The 7AQB-TOM complex showed variations in backbone RMSD till 35 ns ranging from 0.14 to 0.43 nm. The first stable conformation was attained in the time period between 36-50 ns with no considerable deviations in the values (Figure 8). This clearly specifies that the protein underwent small structural changes in all the complexes during simulations.

RMSF is an another crucial parameter while examining the stability and flexibility of complex systems during simulation [39]. RMSF was examined to analyse the change in behaviour of amino acid residues of target protein on binding to a ligand[40,41]. The RMSF values for Cα atoms of the protein were calculated and plotted with respect to the residues. In case of all complex, the amino acid residues showed minimal fluctuations throughout the simulation. The amino acids of MAPK which interacted with ASA during docking showed minimal fluctuation values during MD simulation *viz*. CYS28, GLY29, LYS185 and LYS229, with NAR it showed low fluctuation values during MD simulation *viz* GLY29 and LEU192, with RUT showed minimal fluctuation values during MD simulation *viz*. GLY29, ARG70, LYS229 and ASN269 and with TOM it showed moderate fluctuation values during MD simulation *viz.* GLY29, LYS185, SER189, TYR266 and PRO301 (Figure 9). These results reveal that binding of both the ligands actuated no major effects on the flexibility of the residues in the protein.

Further, Radius of gyration (Rg) of the complex systems were also analysed. Rg is the RMS distance of the atoms of the protein from the axis of rotation [41]. It is one among the important parameter that represents the overall change in the protein structure compactness and its dimensions during the simulation[42]. Higher Rg values characterize the protein as less compact and flexible while low values depict the high compactness and rigidity[39]. Rg values of backbone atoms of protein were plotted against time to examine the changes in structural compactness. Binding of ASA decreased the backbone Rg values till 30 ns. In the time period between 31-50 ns there were no considerable fluctuations and almost constant value of ~1.98 nm was maintained. Till end, the Rg values were found to be in the range between 1.95-1.99 nm. Complete analysis revealed that, in the initial stage the trajectory had shown its peak value of ~2.12 nm. Later this high value was never displayed again which shows the stability of protein in the complex (Figure 10). Binding of NAR decreased the backbone Rg values till 15 ns. In

the time period between 16-45 ns there were no considerable fluctuations and almost constant value of ~2.04 nm was maintained. Till end, the Rg values were found to be in the range of 2.02-2.05 nm. Complete analysis revealed that, in the initial stage, the trajectory showed its peak value of ~2.09 nm. Later, this high value was never displayed again which shows the stability of protein in the complex (Figure 10). Binding of RUT decreased the backbone Rg values till 31 ns. In the time period between 32-50 ns there were no considerable fluctuations and almost constant value of ~2.03 nm was maintained. Till end, the Rg values were found to be in the range of 2.00-2.05 nm. Complete analysis revealed that, in the initial stage, the trajectory exhibited its peak value of ~2.10 nm. Later, this high value was never displayed again which shows the stability of protein in the complex (Figure 10). Binding of TOM decreased the backbone Rg values till 10 ns. In the time period between 11-50 ns there were no considerable fluctuations and almost constant value of ~1.96 nm was maintained. Till end, the Rg values were found to be in the range of 1.94-2.00 nm. Complete analysis revealed that, in the initial stage, the trajectory had shown its peak value of ~2.10 nm. Later, this high value was never displayed again which shows the stability of protein in the complex (Figure 10). The complete interpretation revealed that both the molecules induced no major structural changes in the protein.

Moreover, analysis of Solvent Accessible Surface Area (SASA) for all the complexes was implemented. SASA is the substantial criterion to examine the extent of exposure of receptor to the surrounding solvent molecules during simulation[39,43]. In general, binding of ligand may induce the structural changes in the receptor and hence the area in contact with the solvent also may vary[41]. SASA values of protein was plotted against time to estimate the changes in surface area. For SASA complex, the trajectory showed decrease in the values till 15 ns. Except few time intervals, minute fluctuations were observed throughout the simulation period (Figure 11). The average SASA value was found to be ~138 $nm^2$ and were in the range of 150-130 $nm^2$. For NAR complex, the trajectory showed decrease in the values till 10 ns. Except few time intervals, minute fluctuations were observed throughout the simulation period (Figure 11). The average SASA value was found to be ~142 $nm^2$ and were in the range of 149-134 $nm^2$. For RUT complex, the trajectory showed decrease in the values till 10 ns. In the time interval of 11-28 ns, minute fluctuations were observed and from 29-34 ns a moderate fluctuation was observed (Figure 11). The average SASA value was found to be ~140 $nm^2$ and were in the range of 154-133 $nm^2$. For TOM complex, the trajectory showed decrease in the values till 10 ns. Except few time intervals, minute fluctuations were observed throughout the simulation period (Figure 11). The average SASA value was found to be ~148 $nm^2$ and were in the range of 154-140 $nm^2$. Overall, analysis revealed that the surface area of protein in both complexes were shrunken during the simulation.

To examine the binding affinity of the ligands with the target protein, the MD trajectories were analyzed to interpret the extent of hydrogen bond formation during the entire course of simulation and was depicted in Figure 12. SASA had formed good number of H-bonds with the receptor protein with a maximum of five bonds at several time frames indicating the stronger affinity towards the target. Consistency was maintained in forming almost two hydrogen bonds for the entire simulation time which signifies the stability of the complex. For the NAR complex, the consistency was maintained in forming three hydrogen bonds with maximum of six bonds at certain time periods. For rutin complex, the consistency was maintained in forming four hydrogen bonds with maximum of nine bonds at certain time periods. For the TOM complex, the consistency was maintained in forming two hydrogen bonds with maximum of nine bonds at certain time periods. This clearly signifies that the top phytochemicals have the stronger affinity with the target protein.

## Discussion

The purpose of this research work was to look at the cancer-preventive impact of bioactive chemicals found in the south Indian cuisine *rasam* by using graph theoretical network and pharmacoinformatics analysis. Pharmacoinformatics is a collection of *in silico* molecular modeling tools for screening the bioactive substances based on their binding affinities, pharmacokinetics, and pharmacodynamic features[44]. By enabling researchers to narrow down the biological and synthetic research impacts, pharmacoinformatics has sped up the discovery of bioactive substances. Several substances have their positive effects predicted using pharmacoinformatics research, which were then validated by *in vitro* and *in vivo* activities. Understanding how chemicals bind, interact, and inhibit / stimulate a certain protein might help researchers find therapeutic options for certain disease conditions.

Initially, a graph theoretical network was developed using centrality metrics, and it was suggested for metabolic networks that included enzymatic cascades and synergistic ligand-enzyme interactions. Biological networks, which are made up of a number of vertices (or nodes) linked in a pattern by a set of edges (or connections), are designed to mimic the structure of genuine biological systems. MAPK was identified as a receptor (target) for ligand (bioactive substances) binding in ROS-induced oxidative stress that leads to malignancies, according to the network analysis study. MAPK pathways have been shown to be impacted not just by receptor ligand interactions, but also by various cell stresses. Furthermore, since MAPK pathways regulate both mitogen- and stress-activated signals, the regulation of both pathways by ROS has piqued researchers' attention[45]. The goal of the current research work was to look into the detoxification / neutralization of ROS by employing bioactive chemicals found in *rasam* spices to protect cells against cancer. A total of sixty-six bioactive compounds were chosen from twelve spices using the IMPART database, as well as previously published publications on their effects against different human malignancies. All the chemicals chosen were docked against MAPK protein kinases, with binding affinity ranging from − 3.50 kcal/mol to -10.60 kcal/mol. Four

compounds (Assafoetidinol A (-9.80 kcal/mol), Naringin (-9.60 kcal/mol), Rutin (-9.80 kcal/mol), and Tomatine (-10.60 kcal/mol)) have been chosen for future analysis based on their significant binding affinity, strong hydrophobic and hydrogen bonding interactions with amino acid residues present in the active site of MAPK protein.

A substance's bioactivity is largely governed by its absorption, distribution, metabolism, and excretion (ADME) characteristics, all of which are connected to its pharmacokinetic characteristics. The bioavailability of dietary phytochemicals to target cells, as well as their absorption and metabolism in the human body are certain key aspects in promoting their bioactivity and maintaining body health[46]. The small intestine absorbs some, but not all, of the components of dietary phytochemicals into the circulatory system. Some phytochemical compounds that were absorbed by the colon and altered by the gut microbiota and microbial metabolites were released back into the circulation and showed significant activity[47]. In order for any molecule to permeate the membrane, phytochemicals / test substance must break hydrogen bonds in the aqueous environment and partition across the membrane[48]. The polar surface area (PSA) of a chemical is connected to its hydrogen-bonding potential, whereas molecular mass and lipophilicity are associated to membrane permeability[49]. As a consequence, the ADME properties must be assessed at the earlier stages of drug design and discovery process in order to pass the standard clinical studies required to be considered as prospective therapeutic candidate[50]. In this study, all the discovered phytoconstituents were confirmed in terms of usual pharmacokinetic properties using multiple bioinformatics methods. Phytochemicals are naturally derived from variety of plants that are often consumed by humans and are usually considered safe to consume. While most phytochemicals are not regulated by the Food and Drug Administration (FDA) in the United States, their potential toxicity is unknown.

Phytochemicals are utilized as supplements in conjunction with illness therapy all around the world, but do not necessarily inform to their physicians of their use[51]. Substance toxicity refers to the property of any compound to be poisonous and to cause harm to an organism. Toxicity testing of a substance necessitates *in vitro* and *in vivo* animal experiments, which is time-consuming, expensive, and complicated technique. Because there are no animal trials, precision, accessibility, and speed. Hence, *in silico* toxicity assessment has become very popular in recent times and it can offer information on any synthetic or natural molecule. In this work, *in silico* approaches were used to estimate the toxicity levels of four chemicals. The non-carcinogenic and non-skin irritating properties of four substances were determined using *in silico* testing. Three compounds, Assafoetidinol A, Rutin, and Tomatine were shown to be negative in Ames testing. Toxicity tests revealed that the four phytochemicals chosen had no negative side effects (hERG). The $LD_{50}$ (median fatal dosage) indicates the immediate or acute toxicity of substances that were determined to be the most effective in the investigation. Hence, the complexes of these compounds were subjected to molecular dynamics simulations and the results were analysed with the results of apo form of MAPK (7AQB). The complexes were validated by interpreting the RMSD, RMSF, Rg, SASA and the lead phytochemical complexes were found to be stable during the simulations.

## Conclusion

Traditionally, home-cooked meals have been shown to help avoid chronic illnesses, improve health, and save treatment costs while also boosting quality of life. This study looked at the antioxidant properties of bioactive chemicals found in the south Indian cuisine *rasam* against oxidative stress-induced human malignancies. In the human body, ROS is a metabolic by-product of cellular respiration. Oxidative stress and overexpression of MAPK protein are caused by an increase in ROS levels. MAPK overexpression causes a cascade of events in cells, including mutations and carcinogenesis. Through a thorough pharmacoinformatics-based molecular docking investigation of bioactive substances against MAPK, the antioxidant potential of *rasam* has been proven in the current work. *In silico* molecular docking investigations found that the four lead phytochemicals (Assafoetidinol A, Naringin, Rutin, and Tomatine) may suppress MAPK expression. In addition, MD stimulation tests and *in silico* pharmacokinetic prediction analyses gives the safety profile of four lead compounds as well as the stability of the protein-ligand complex, although, in order to determine the *rasam*'s effectiveness, further *in vitro* and *in vivo* animal research work will be necessary.

## Declarations


### Acknowledgements

The authors are grateful to the Management of Kalasalingam Academy of Research and Education, Krishnankoil, Tamilnadu, India, for utilizing research facilities.


### Ethics Approval and Consent to Participate

Not applicable.

### Human and Animal Rights

No Animals/Humans were used for studies that are base of this research.

### Consent for Publication

Not applicable.

### Funding

None.

### Conflict of Interest

The authors declare no conflict of interest, financial or otherwise.

## References

1. Kunjiappan, S. *et al.* Capsaicin-loaded solid lipid nanoparticles: design, biodistribution, in silico modeling and in vitro cytotoxicity evaluation., **32**, 095101 (2020).
2. Sung, H. *et al.* Global cancer statistics 2020: GLOBOCAN estimates of incidence and mortality worldwide for 36 cancers in 185 countries. *CA: a cancer journal for clinicians*, **71**, 209–249 (2021).
3. Kushi, L. H. *et al.* American Cancer Society Guidelines on nutrition and physical activity for cancer prevention: reducing the risk of cancer with healthy food choices and physical activity. *CA: a cancer journal for clinicians*, **62**, 30–67 (2012).
4. Perše, M. The Role of the Antioxidant Defense System in the Pathogenesis of Colorectal Cancer.*FREE RADICALS*;217.
5. Ren, J., Sowers, J. R. & Zhang, Y. *Autophagy and Cardiometabolic Diseases: From Molecular Mechanisms to Translational Medicine* (Academic Press, 2018).
6. Kunjiappan, S. *et al.* Design, in silico modelling and functionality theory of folate-receptor-targeted myricetin-loaded bovine serum albumin nanoparticle formulation for cancer treatment. Nanotechnology 31, 155102(2020).
7. Palmeira, C. M. *et al.* Mitohormesis and metabolic health: The interplay between ROS, cAMP and sirtuins. *Free Radical Biology and Medicine*, **141**, 483–491 (2019).
8. Nordberg, J. & Arnér, E. S. Reactive oxygen species, antioxidants, and the mammalian thioredoxin system. *Free radical biology and medicine*, **31**, 1287–1312 (2001).
9. Ganesan, V. *et al.* Optimization and analysis of microwave-assisted extraction of bioactive compounds from Mimosa pudica L. using RSM & ANFIS modeling. *Journal of Food Measurement and Characterization*, **12**, 228–242 (2018).
10. Sachdev, S., Ansari, S. A., Ansari, M. I., Fujita, M. & Hasanuzzaman, M. Abiotic stress and reactive oxygen species: Generation, signaling, and defense mechanisms. *Antioxidants*, **10**, 277 (2021).
11. Mates, J. Effects of antioxidant enzymes in the molecular control of reactive oxygen species toxicology., **153**, 83–104 (2000).
12. Xiao, H., Lü, F., Stewart, D. & Zhang, Y. Mechanisms underlying chemopreventive effects of flavonoids via multiple signaling nodes within Nrf2-ARE and AhR-XRE gene regulatory networks. *Curr. Chem. Biol*, **7**, 151–176 (2013).
13. Sachan, A., Kumar, S., Kumari, K. & Singh, D. Medicinal uses of spices used in our traditional culture: Worldwide. *Journal of Medicinal Plants Studies*, **6**, 116–122 (2018).
14. Zheng, J. *et al.* Spices for prevention and treatment of cancers. *Nutrients*, **8**, 495 (2016).
15. Tamvakopoulos, C. *et al.* Metabolism and anticancer activity of the curcumin analogue, dimethoxycurcumin. *Clin. Cancer Res*, **13**, 1269–1277 (2007).
16. Raza, K. *et al.* Conjugation of docetaxel with multiwalled carbon nanotubes and codelivery with piperine: implications on pharmacokinetic profile and anticancer activity. *Molecular pharmaceutics*, **13**, 2423–2432 (2016).
17. Sharoni, Y., Danilenko, M. & Levy, J. Molecular mechanisms for the anticancer activity of the carotenoid lycopene. *Drug development research*, **50**, 448–456 (2000).
18. Mohan, U. P. *et al.* Utilization of plant-derived Myricetin molecule coupled with ultrasound for the synthesis of gold nanoparticles against breast cancer. *Naunyn-Schmiedeberg's Archives of Pharmacology*, **393**, 1963–1976 (2020).
19. Pandian, S. R. K. *et al.* Formulation and evaluation of rutin-loaded solid lipid nanoparticles for the treatment of brain tumor. *Naunyn-Schmiedeberg's Archives of Pharmacology*, **394**, 735–749 (2021).
20. Sheen, B. *Foods of India* (Greenhaven Publishing LLC, 2006).
21. Devarajan, A. & Mohanmarugaraja, M. A comprehensive review on Rasam: A South Indian traditional functional food. *Pharmacognosy reviews*, **11**, 73 (2017).
22. Bélanger, J. *Green Leafy Vegetables of Rural India: Ethnobotany and* (McGill University, 2010).

23. Wang, S., Meckling, K. A., Marcone, M. F., Kakuda, Y. & Tsao, R. Synergistic, additive, and antagonistic effects of food mixtures on total antioxidant capacities. *Journal of agricultural and food chemistry*, **59**, 960–968 (2011).
24. Pan, M. H. & Ho, C. T. Chemopreventive effects of natural dietary compounds on cancer development. *Chem. Soc. Rev*, **37**, 2558–2574 (2008).
25. Dreosti, I. E. Bioactive ingredients: antioxidants and polyphenols in tea. *Nutrition reviews*, **54**, S51–S58 (1996).
26. Kunjiappan, S. *et al.* Design graph theoretical analysis and in silico modeling of dunaliella bardawil biomass encapsulated N-succinyl chitosan nanoparticles for enhanced anticancer activity. *Anti-Cancer Agents in Medicinal Chemistry (Formerly Current Medicinal Chemistry-Anti-Cancer Agents)*, **18**, 1900–1918 (2018).
27. Theivendren, P. *et al.* Graph theoretical analysis, insilico modeling and formulation of pyrimidine nanoparticles as p38α MAP kinases inhibitors: a quantitative proteomics approach. *Drug research*, **69**, 100–110 (2019).
28. Saravanan, G. *et al.* Design, graph theoretical analysis, density functionality theories, Insilico modeling, synthesis, characterization and biological activities of novel thiazole fused quinazolinone derivatives. *Drug development research*, **79**, 260–274 (2018).
29. Berman, H. M. *et al.* The protein data bank. *Nucleic acids research*, **28**, 235–242 (2000).
30. Mohanraj, K. *et al.* IMPPAT: A curated database of Indian medicinal plants, phytochemistry and therapeutics. bioRxiv, 206995(2017).
31. Dallakyan, S. & Olson, A. J. in Chemical biology 243–250(Springer, 2015).
32. Gaillard, T. Evaluation of AutoDock and AutoDock Vina on the CASF-2013 benchmark. *Journal of chemical information and modeling*, **58**, 1697–1706 (2018).
33. Mohan, U. P., Kunjiappan, S., Pichiah, P. T. & Arunachalam, S. Adriamycin inhibits glycolysis through downregulation of key enzymes in Saccharomyces cerevisiae. *3 Biotech*, **11**, 1–13 (2021).
34. Wang, Y. *et al.* In silico prediction of human intravenous pharmacokinetic parameters with improved accuracy. *Journal of chemical information and modeling*, **59**, 3968–3980 (2019).
35. Jia, C. Y., Li, J. Y., Hao, G. F. & Yang G.-F. A drug-likeness toolbox facilitates ADMET study in drug discovery., **25**, 248–258 (2020).
36. Markov, S., Petkov, P. & Pavlov, V. in *International conference on Variability of the Sun and sun-like stars: from asteroseismology to space weather.* 359–367 (Springer).
37. Van Aalten, D. M. *et al.* PRODRG, a program for generating molecular topologies and unique molecular descriptors from coordinates of small molecules. *Journal of computer-aided molecular design*, **10**, 255–262 (1996).
38. Sharma, A., Datta, D. & Balasubramaniam, R. Molecular dynamics simulation to investigate the orientation effects on nanoscale cutting of single crystal copper. *Comput. Mater. Sci*, **153**, 241–250 (2018).
39. Kumar, B., Parasuraman, P., Murthy, T. P. K., Murahari, M. & Chandramohan, V. In silico screening of therapeutic potentials from Strychnos nux-vomica against the dimeric main protease (Mpro) structure of SARS-CoV-2.*Journal of Biomolecular Structure and Dynamics*,1–19(2021).
40. Abdelrheem, D. A. *et al.* The inhibitory effect of some natural bioactive compounds against SARS-CoV-2 main protease: insights from molecular docking analysis and molecular dynamic simulation. *Journal of Environmental Science and Health, Part A*, **55**, 1373–1386 (2020).
41. Rahman, M. M. *et al.* Virtual screening, molecular dynamics and structure–activity relationship studies to identify potent approved drugs for Covid-19 treatment.*Journal of Biomolecular Structure and Dynamics*,1–11(2020).
42. Gupta, S. *et al.* Identification of potential natural inhibitors of SARS-CoV2 main protease by molecular docking and simulation studies.*Journal of Biomolecular Structure and Dynamics*,1–12(2020).
43. Ghosh, S. K., Saha, B. & Banerjee, R. Insight into the sequence-structure relationship of TLR cytoplasm's Toll/Interleukin-1 receptor domain towards understanding the conserved functionality of TLR 2 heterodimer in mammals.*Journal of Biomolecular Structure and Dynamics*,1–10(2020).
44. Alamri, M. A. Pharmacoinformatics and molecular dynamic simulation studies to identify potential small-molecule inhibitors of WNK-SPAK/OSR1 signaling that mimic the RFQV motifs of WNK kinases. *Arabian Journal of Chemistry*, **13**, 5107–5117 (2020).
45. Yang, K. Y., Liu, Y. & Zhang, S. Activation of a mitogen-activated protein kinase pathway is involved in disease resistance in tobacco. Proceedings of the national academy of sciences 98, 741–746(2001).
46. da Silva, B. V., Barreira, J. C. & Oliveira, M. B. P. Natural phytochemicals and probiotics as bioactive ingredients for functional foods: Extraction, biochemistry and protected-delivery technologies. *Trends in Food Science & Technology*, **50**, 144–158 (2016).
47. Giampieri, F. *et al.* The strawberry: Composition, nutritional quality, and impact on human health. *Nutrition*, **28**, 9–19 (2012).
48. Selby-Pham, S. N., Miller, R. B., Howell, K., Dunshea, F. & Bennett, L. E. Physicochemical properties of dietary phytochemicals can predict their passive absorption in the human small intestine. *Scientific reports*, **7**, 1–15 (2017).

49. Alex, A., Millan, D. S., Perez, M., Wakenhut, F. & Whitlock, G. A. Intramolecular hydrogen bonding to improve membrane permeability and absorption in beyond rule of five chemical space. *MedChemComm*, **2**, 669–674 (2011).
50. Hughes, J. P., Rees, S., Kalindjian, S. B. & Philpott, K. L. Principles of early drug discovery. *British journal of pharmacology*, **162**, 1239–1249 (2011).
51. Sen, S. & Chakraborty, R. Revival, modernization and integration of Indian traditional herbal medicine in clinical practice: Importance, challenges and future. *Journal of traditional and complementary medicine*, **7**, 234–244 (2017).

## Tables

Table 1: The nodes and edges of influential protein (MAPK)

| Centrality measures | Maximum | Mean | Minimum |
|---|---|---|---|
| Betweenness | 498.93 | 93.517625 | 1 |
| Closeness | 15.49 | 6.73 | 1 |
| Degree | 16 | 4.4107 | 2 |
| Eigenvector | 0.356462577 | 0.08 | 0.0001 |
| Eccentricity | 1 | 0.381 | 0.11 |
| Radiality | 9.18 | 7.86 | 5.08 |
| Stress | 1256 | 342.18 | 1 |
| Nodes | 129 | | |
| Edges | 177 | | |

Table 2: The results of threshold parameter values of the network analysis

| Rank | Gene | Degree | Betweenness | Closeness | Eccentricity | Eigen Vector | Radiality | Stress |
|---|---|---|---|---|---|---|---|---|
| 1 | K04441 | 16 | 498.93 | 13.83 | 0.33 | 0.232772 | 8.16 | 1256 |
| 2 | K04440 | 15 | 235.5 | 6 | 1 | 0.356463 | 8.75 | 492 |
| 2 | K02833 | 12 | 433.43 | 11.95 | 0.2 | 0.188387 | 8.81 | 2094 |
| 3 | K04371 | 13 | 322.57 | 8.5 | 0.5 | 0.16084 | 8.11 | 1830 |
| 4 | K04416 | 11 | 451.4 | 12.58 | 0.25 | 0.297805 | 9.43 | 1328 |
| 5 | K04427 | 8 | 238 | 10.95 | 0.2 | 0.116981 | 8.79 | 683 |
| 6 | K04430 | 8 | 158.75 | 7 | 0.5 | 0.254947 | 9.18 | 309 |
| 7 | K04431 | 8 | 33.83 | 6 | 0.5 | 0.219992 | 8.64 | 43 |
| 9 | K04433 | 7 | 232.47 | 8.25 | 0.25 | 0.146817 | 8.75 | 625 |
| 10 | K04432 | 7 | 232.47 | 8.25 | 0.25 | 0.146817 | 8.79 | 625 |
| 11 | K04369 | 7 | 170.78 | 6.33 | 0.33 | 0.199213 | 8.8 | 1068 |
| 12 | K04368 | 7 | 170.78 | 6.33 | 0.33 | 0.199213 | 8.78 | 1068 |
| 13 | K04426 | 6 | 198.93 | 7.45 | 0.2 | 0.094722 | 8.91 | 436 |
| 14 | K04436 | 5 | 83.58 | 4 | 0.5 | 0.241424 | 9.08 | 224 |
| 15 | K03173 | 5 | 106.3 | 17.52 | 0.16 | 0.093952 | 9.16 | 279 |
| 16 | K04467 | 5 | 32 | 1 | 1 | 0.12377 | 8.98 | 48 |
| 17 | K04466 | 4 | 6 | 2 | 1 | 0.075752 | 8.58 | 17 |
| 18 | K04366 | 4 | 72.37 | 5.97 | 0.25 | 0.124896 | 8.16 | 494 |
| 19 | K04365 | 4 | 75.93 | 5.97 | 0.25 | 0.117484 | 8.12 | 520 |
| 20 | K04403 | 4 | 120 | 7.93 | 0.16 | 0.045093 | 8.63 | 334 |
| 21 | K03175 | 4 | 108 | 8.71 | 0.14 | 0.014636 | 7.8 | 380 |
| 22 | K02187 | 4 | 46.7 | 11.45 | 0.2 | 0.071373 | 8.58 | 150 |
| 23 | K04434 | 4 | 9.33 | 4 | 0.5 | 0.145212 | 7.91 | 14 |
| 24 | K04419 | 4 | 2 | 5.5 | 0.33 | 0.126663 | 8.27 | 2 |
| 25 | K04378 | 4 | 1 | 1 | 1 | 0.039866 | 7.24 | 1 |
| 26 | C00076 | 3 | 32 | 8.59 | 0.14 | 0.01566 | 6.99 | 260 |
| 27 | K02677 | 3 | 29.5 | 10.37 | 0.2 | 0.062884 | 8.04 | 51 |
| 28 | K04345 | 3 | 5.57 | 4.43 | 0.16 | 0.009074 | 6.4 | 30 |
| 29 | K04443 | 3 | 31.75 | 2 | 1 | 0.052187 | 7.19 | 142 |
| 30 | K04428 | 3 | 19 | 7.45 | 0.2 | 0.058613 | 7.79 | 40 |
| 31 | K02308 | 3 | 80 | 6.1 | 0.16 | 0.019723 | 8.01 | 164 |
| 32 | K04409 | 3 | 5 | 1 | 1 | 0.026699 | 7.66 | 5 |
| 33 | K03171 | 3 | 106 | 15.49 | 0.14 | 0.03305 | 8.31 | 290 |
| 34 | K08845 | 3 | 47.37 | 5.92 | 0.25 | 0.112807 | 8.16 | 442 |
| 35 | K04349 | 2 | 30 | 8.93 | 0.16 | 0.039225 | 7.92 | 258 |
| 36 | K04353 | 2 | 17.567 | 4.87 | 0.2 | 0.024329 | 7.28 | 55 |
| 37 | K08018 | 2 | 26.93 | 8.93 | 0.16 | 0.037953 | 7.89 | 129 |
| 38 | K08053 | 2 | 30 | 8.93 | 0.16 | 0.037605 | 7.87 | 129 |
| 39 | K04350 | 2 | 30 | 8.93 | 0.16 | 0.039225 | 7.91 | 258 |

| | | | | | | | | |
|---|---|---|---|---|---|---|---|---|
| 40 | K03099 | 2 | 90 | 8.93 | 0.16 | 0.037662 | 7.91 | 387 |
| 41 | K04364 | 2 | 62 | 7.59 | 0.14 | 0.007529 | 7.01 | 260 |
| 42 | K04361 | 2 | 32 | 6.81 | 0.12 | 0.001503 | 6.07 | 131 |
| 43 | K04464 | 2 | 34 | 1 | 1 | 0.009289 | 6.37 | 72 |
| 44 | K04463 | 2 | 66 | 1.5 | 0.5 | 0.046533 | 7.31 | 142 |
| 45 | K04445 | 2 | 15.25 | 1 | 1 | 0.048467 | 7.22 | 71 |
| 46 | K04404 | 2 | 60 | 7.93 | 0.16 | 0.025302 | 7.99 | 230 |
| 47 | K04391 | 2 | 25 | 6.71 | 0.14 | 0.009001 | 7.72 | 47 |
| 48 | K04388 | 2 | 21 | 5.46 | 0.14 | 0.003937 | 7.11 | 42 |
| 49 | K04390 | 2 | 21 | 5.46 | 0.14 | 0.003937 | 7.11 | 42 |
| 50 | K04386 | 2 | 30 | 5.83 | 0.1 | 1.00E-04 | 5.08 | 98 |
| 51 | K03158 | 2 | 54 | 12.43 | 0.12 | 0.006597 | 7.38 | 146 |
| 52 | K04442 | 2 | 16.5 | 1 | 1 | 0.048467 | 7.34 | 71 |
| 53 | K04373 | 2 | 18.25 | 1 | 1 | 0.033387 | 7.14 | 184 |
| 54 | K04372 | 2 | 18.25 | 1 | 1 | 0.033387 | 7.17 | 184 |
| 55 | K04729 | 2 | 58 | 6.28 | 0.11 | 5.85E-04 | 5.99 | 194 |
| 56 | K04730 | 2 | 84 | 7.03 | 0.12 | 0.002926 | 6.9 | 288 |

Table 3: Bioactive compounds in *Rasam* ingredients and their binding affinity against MAPK

| S. No | Ingredients | Compound id (CID) | Bioactive compound name | Docking score (kcal/mol) |
|---|---|---|---|---|
| 1 | Turmeric | 969516 | Curcumin | -7.8 |
| 2 | | 5469424 | Demethoxycurcumin | -7 |
| 3 | | 5315472 | Bisdemethoxycurcumin | -7.7 |
| 4 | | 10250249 | 5'-methoxycurcumin | -6.7 |
| 5 | | 443160 | (+)-Alpha-Phellandrene | -6.6 |
| 6 | | 10429233 | Dihydrocurcumin | -7.2 |
| 7 | | 92776 | Zingiberene | -6.2 |
| 8 | | 10887971 | (+)-Sabinene | -6.6 |
| 9 | | 64685 | Borneol | -5.2 |
| 10 | Red pepper | 1548943 | Capsaicin | -6.1 |
| 11 | | 5281229 | Capsorubin | -8 |
| 12 | | 5281228 | Capsanthin | -8.4 |
| 13 | | 77994099 | Bicyclomahanimbicine | -9.5 |
| 14 | | 107982 | Dihydrocapsaicin | -6.2 |
| 15 | | 448438 | Violaxanthin | -9.4 |
| 16 | Asafoetida | 131751454 | Assafoetidin | -8.3 |
| 17 | | 7067262 | Franesiferol A | -7.3 |
| 18 | | 15559239 | Franesiferol C | -8.9 |
| 19 | | 11892267 | Conferol | -9.2 |
| 20 | | 12041593 | Assafoetidinol A | -9.8 |
| 21 | | 636584 | Assafoetidinol B | -9.5 |
| 22 | Cumin | 95779 | Thymohydroquinone | -6 |
| 23 | | 637563 | *t*-anethole | -6.1 |
| 24 | | 6989 | Thymol | -6.8 |
| 25 | | 5282799 | Dihomolinoleic acid | -5.2 |
| 26 | | 985 | Palmitic acid | -5.1 |
| 27 | Mustard | 370 | Gallic acid | -5.8 |
| 28 | | 5280343 | Quercetin | -8.1 |
| 29 | | 5280805 | Rutin | -9.8 |
| 30 | | 689043 | Caffeic acid | -6.4 |
| 31 | | 445858 | Ferulic acid | -6.5 |
| 32 | | 637542 | *p*-Coumaric acid | -6.6 |
| 33 | | 1183 | Vanillin | -6.1 |
| 34 | | 65064 | (-)-Epigallocatechin Gallate | -8.9 |
| 35 | | 107905 | (-)-Epicatechin Gallate | -9.5 |
| 36 | | 442428 | Naringin | -9.6 |
| 37 | | 5281855 | Ellagic Acid | -8.3 |
| 38 | Sesame oil | 101746 | Sesamolin | -9.4 |
| 39 | | 94672 | Sesaminol | -9.5 |

| | | | | |
|---|---|---|---|---|
| 40 | | 5281235 | Beta-Cryptoxanthin | -8.7 |
| 41 | | 135404715 | Hydroxysesamone | -7.2 |
| 42 | | 360837 | 2,3-epoxysesamone | -7.8 |
| 43 | | 72307 | Sesamin | -9.4 |
| 44 | Black pepper | 971 | Oxalic acid | -3.8 |
| 45 | | 10364 | Carvacrol | -6.5 |
| 46 | | 5318825 | Koenigine | -8.2 |
| 47 | | 278055 | Koenigicine | -7.7 |
| 48 | | 59053143 | Murrayastine | -7.5 |
| 49 | | 398941 | Dithymoquinone | -3.3 |
| 50 | Coriander | 10282 | Monoterpene | -6.3 |
| 51 | | 6549 | Linalool | -4.8 |
| 52 | | 1549026 | Geranyl acetate | -5.3 |
| 53 | | 6654 | α-pinene | -5.5 |
| 54 | Tamarind | 875 | Tartaric acid | -5.1 |
| 55 | Garlic | 65036 | Allicin | -4.4 |
| 56 | | 16590 | Diallyl disulfide | -3.5 |
| 57 | | 16315 | Diallyl trisulfide | -3.6 |
| 58 | | 5386591 | Ajoene | -4.2 |
| 59 | | 9793905 | S-allyl-cysteine | -4.4 |
| 60 | Fenugreek | 5570 | Trigonelline | -5.5 |
| 61 | | 354616 | Gentianine | -6.1 |
| 62 | | 444170 | Fenugreekine | -8.5 |
| 63 | | 5280441 | VitexinLThymo | -8.9 |
| 64 | Tomato | 446925 | Lycopene | -7.4 |
| 65 | | 28523 | Tomatine | -10.6 |
| 66 | | 54670067 | Ascorbic acid | -5.7 |

**Table 4**. List of bonding interactions between selected four phytochemical with MAPK

| Compounds | Residues | AA | Distance (Å) | Bond category |
|---|---|---|---|---|
| CID: 2041593 Assafoetidinol A | 110A | TYR | 3.81 | Hydrophobic |
| | 120B | GLU | 3.57 | Hydrophobic |
| | 163A | GLU | 3.74 | Hydrophobic |
| | 196B | TRP | 3.86 | Hydrophobic |
| | 110A | TYR | 2.09 | Hydrogen |
| | 112A | GLU | 3.58 | Hydrogen |
| | 156B | ALA | 2.10 | Hydrogen |
| | 161A | ASN | 2.85 | Hydrogen |
| | 154A | LYS | 5.34 | Salt |
| | 45A | ARG | 3.64 | Alkyl |
| | 116B | ALA | 3.75 | Alkyl |
| | 155B | PRO | 3.67 | Pi-alkyl |
| CID: 442428 Naringin | 116B | ALA | 3.84 | Hydrophobic |
| | 154B | LYS | 3.76 | Hydrophobic |
| | 163A | GLU | 3.86 | Hydrophobic |
| | 194A | THR | 3.75 | Hydrophobic |
| | 120B | GLU | 3.22 | Hydrogen |
| | 154B | LYS | 3.11 | Hydrogen |
| | 161A | ASN | 3.99 | Hydrogen |
| | 228B | GLY | 3.04 | Hydrogen |
| CID: 5280805 Rutin | 45A | ARG | 3.64 | Hydrophobic |
| | 163A | GLU | 3.59 | Hydrophobic |
| | 194B | THR | 3.71 | Hydrophobic |
| | 196B | TRP | 3.71 | Hydrophobic |
| | 45A | ARG | 3.84 | Hydrogen |
| | 116B | ALA | 4.03 | Hydrogen |
| | 120B | GLU | 3.10 | Hydrogen |
| | 161A | ASN | 3.20 | Hydrogen |
| | 197B | TYR | 2.93 | Hydrogen |
| | 224B | GLU | 3.44 | Hydrogen |
| CID: 28523 Tomatine | 134A | TYR | 3.97 | Hydrophobic |
| | 166A | VAL | 3.75 | Hydrophobic |
| | 32B | GLY | 3.42 | Hydrogen |
| | 45A | ARG | 3.25 | Hydrogen |
| | 161A | ASN | 4.08 | Hydrogen |
| | 230B | THR | 3.25 | Hydrogen |

**Table 5**. List of pharmacokinetics properties includes physicochemical properties, lipophilicity, water solubility, drug-likeness and medicinal chemistry of selected four compounds

| Properties | | CID: 2041593 Assafoetidinol A | CID: 442428 Naringin | CID: 5280805 Rutin | CID: 28523 Tomatine |
|---|---|---|---|---|---|
| **Physicochemical properties** | Molecular weight (g/mol) | 398.49 | 580.53 | 610.52 | 1431.59 |
| | Heavy atoms | 29 | 41 | 43 | 101 |
| | No. Arom. heavy atoms | 10 | 12 | 16 | 12 |
| | Rotatable bonds | 3 | 6 | 6 | 20 |
| | H-bond acceptors | 5 | 14 | 16 | 29 |
| | H-bond donors | 2 | 8 | 10 | 15 |
| **Lipophilicity** | Log $P_{o/w}$ | 3.61 | 2.38 | 2.43 | 4.51 |
| **Water solubility** | Log S (ESOL) | Moderately soluble | Soluble | Moderately soluble | Moderately soluble |
| **Pharmacokinetics** | GI absorption | High | Low | Low | Low |
| **Drug-likeness** | Lipinski | Yes | No | No | No |
| | Bioavailability score | 0.55 | 0.17 | 0.17 | 0.17 |
| **Medi. Chemistry** | Synth. accessibility | Easy | Easy | Easy | Easy |

**Table 6**. List of the drug-induced hERG inhibition, AMES toxicity, carcinogens, Tetrahymena pyriformis (TP) toxicity, rat acute toxicity ($LD_{50}$ in mol/kg), and skin sensitisation along with Minnow toxicity of selected four compounds

| Compound ID | AMES toxicity | Max. tolerated dose (human) | hERG inhibition | LD50 | Hepatotoxicity | Carcinogenicity | Skin Sensitisation | *T.pyriformis* toxicity | Minnow toxicity |
|---|---|---|---|---|---|---|---|---|---|
| CID: 2041593 Assafoetidinol A | No | -0.448 | No | 2.889 | Yes | No | No | 0.651 | 1.212 |
| CID: 442428 Naringin | Yes | 0.491 | No | 2.652 | No | No | No | 0.285 | 4.999 |
| CID: 5280805 Rutin | No | 0.435 | No | 2.472 | No | No | No | 0.285 | 4.079 |
| CID: 28523 Tomatine | No | 0.216 | No | 2.482 | No | No | No | 0.285 | 13.574 |

# Figures

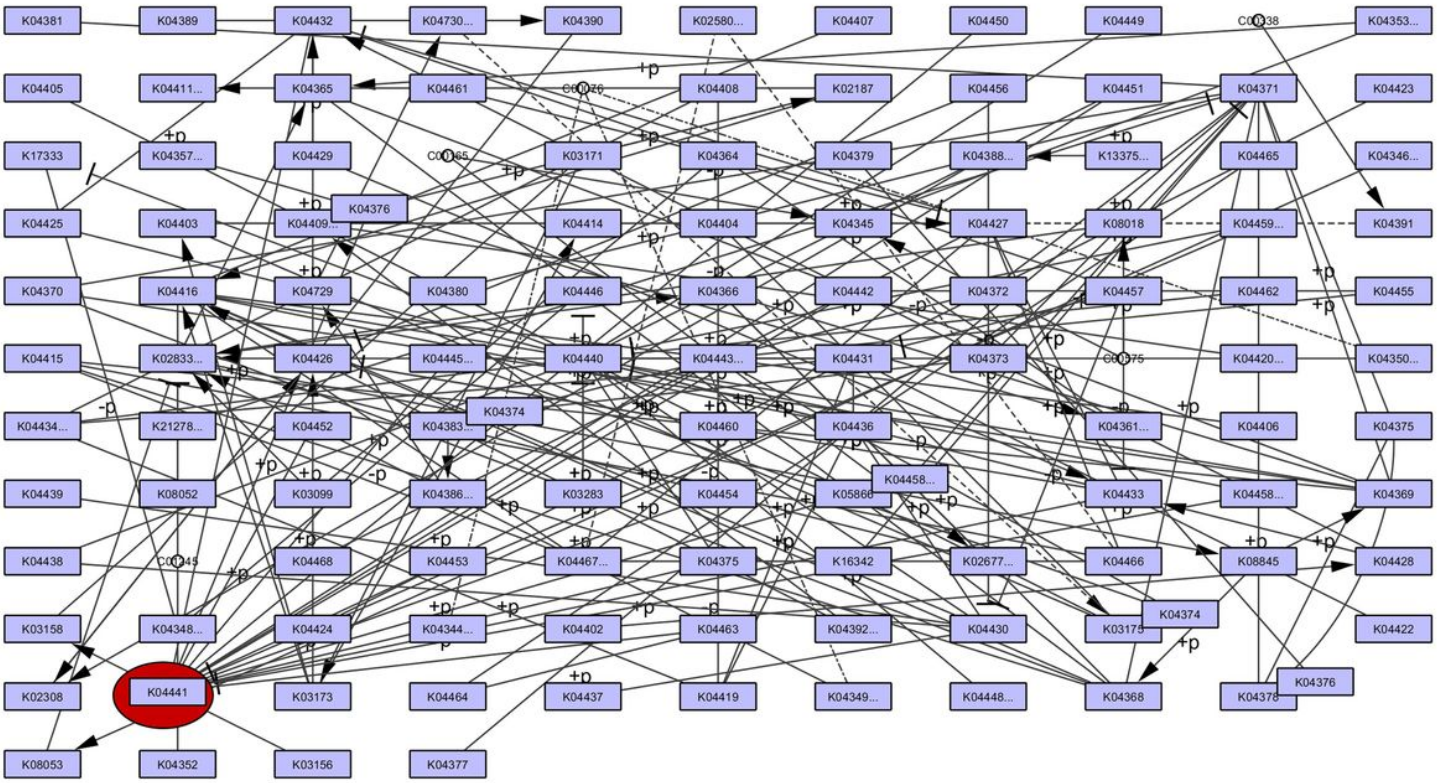


**Figure 1**

The signaling pathway of MAPK

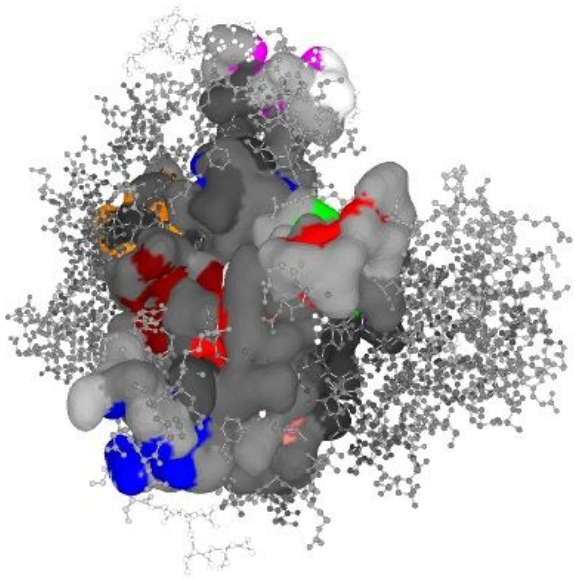

**Figure 2**

Showing active site and correspondence binding site of MAPK.

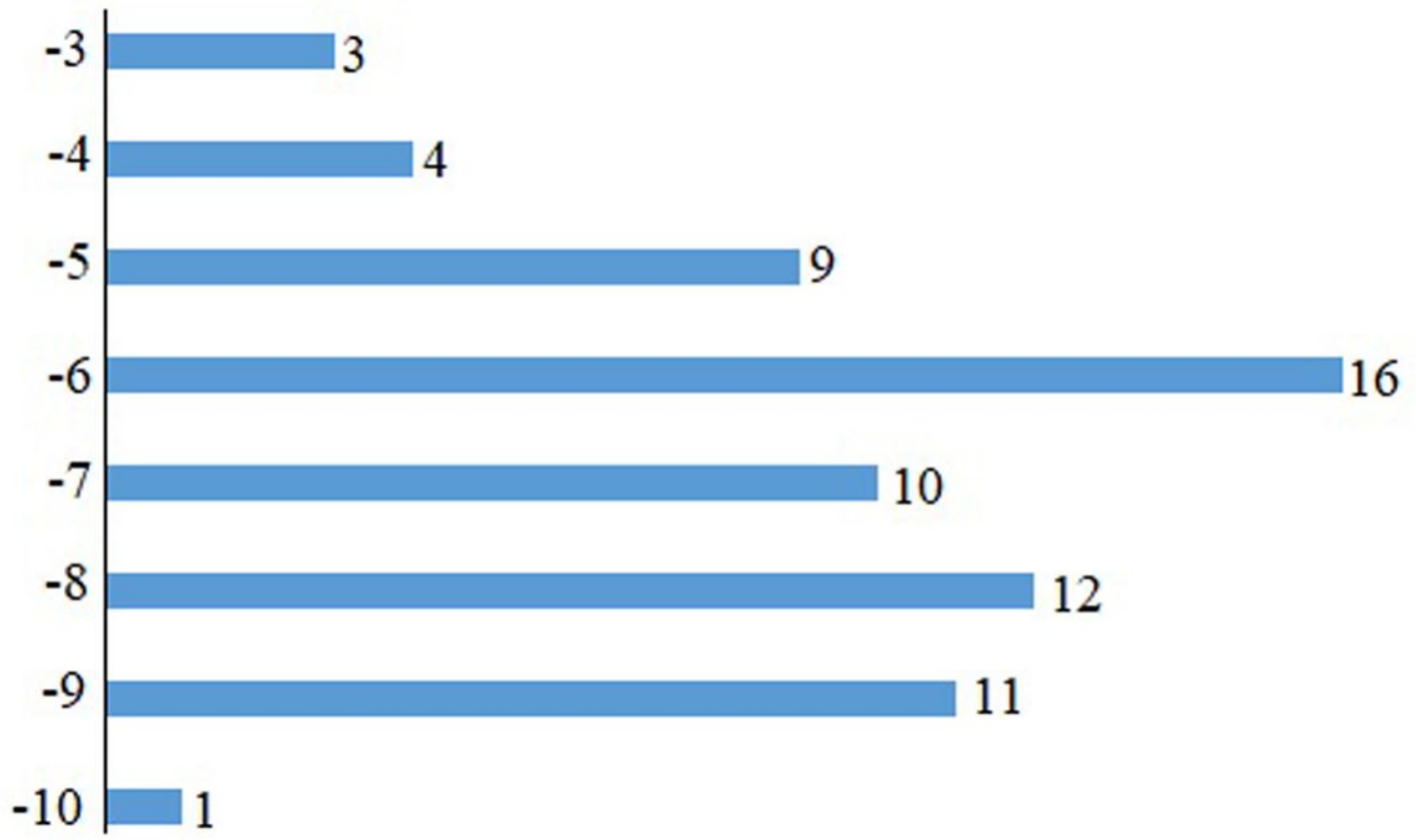


**Figure 3**

Showing the range of docking score distribution of sixty-six phytochemicals presence in the Rasam.

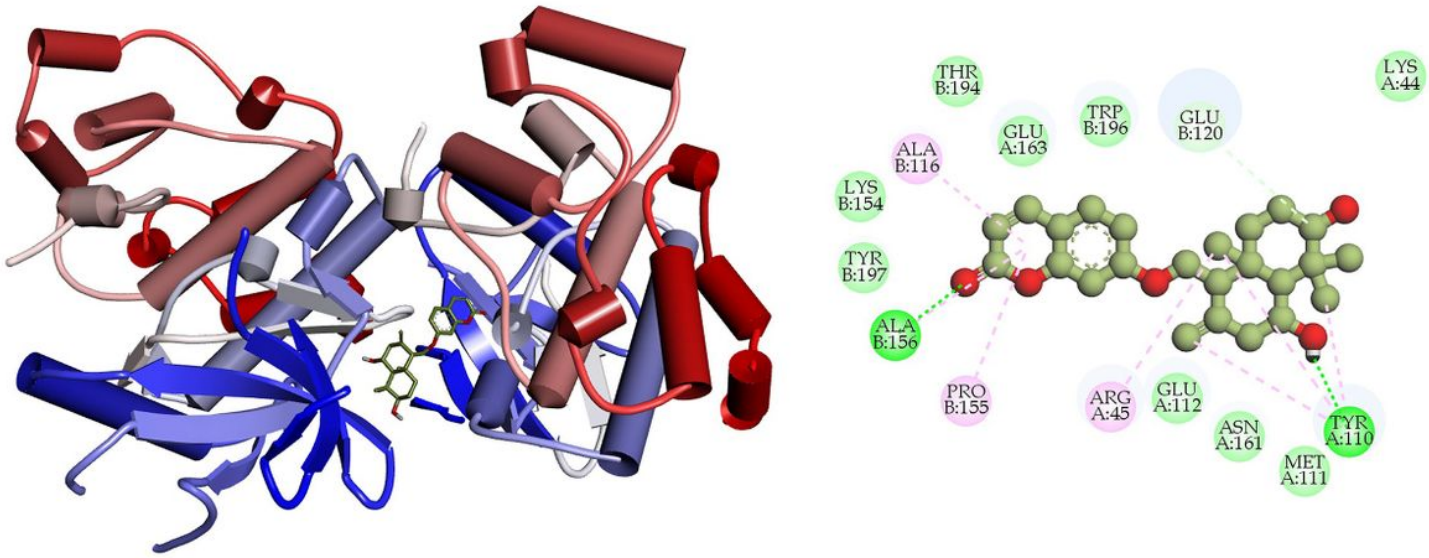


**Figure 4**

Depicted the interaction between the compound CID: 12041593 (Assafoetidinol A) and MAPK. Left side representing 3D and the right side representing 2D complex protein–ligand interaction.

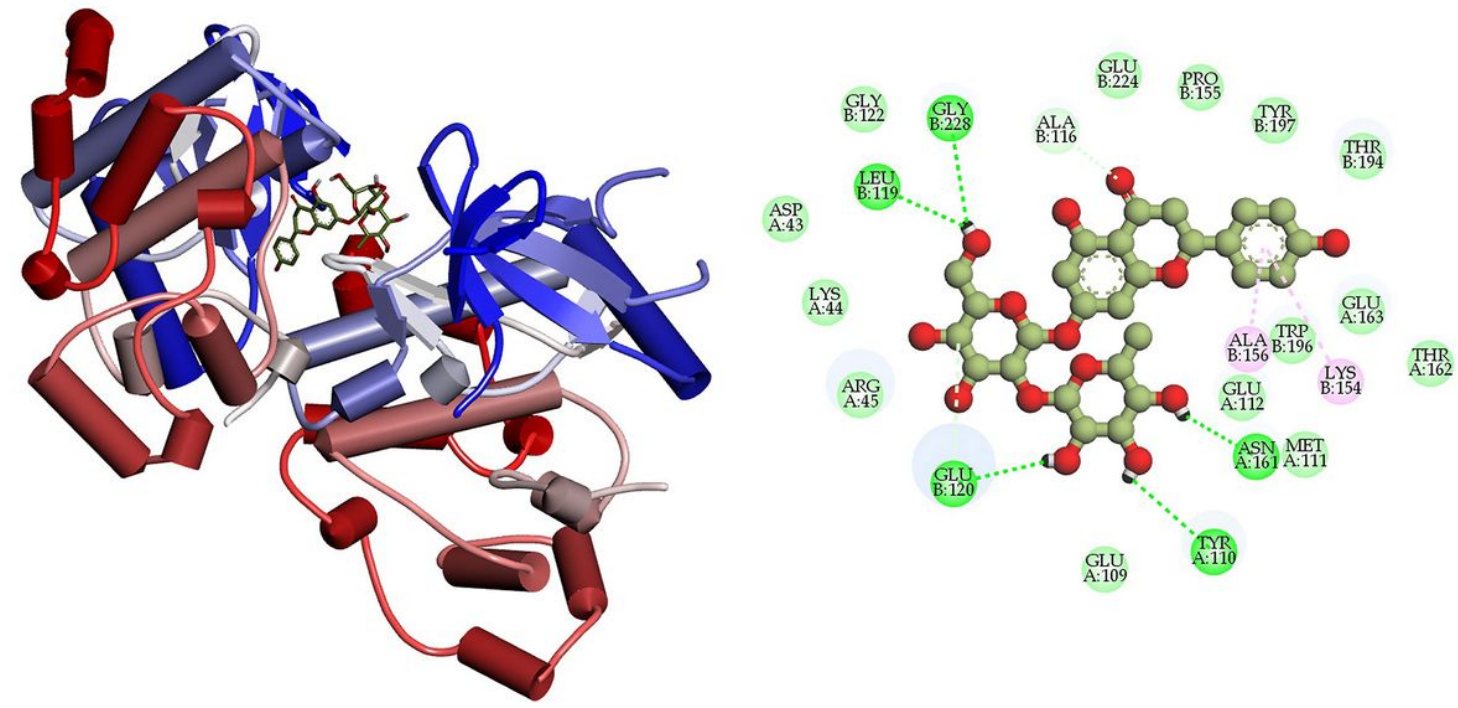


**Figure 5**

Depicted the interaction between the compound CID: 442428 (Naringin) and MAPK. Left side representing 3D and the right side representing 2D complex protein–ligand interaction.

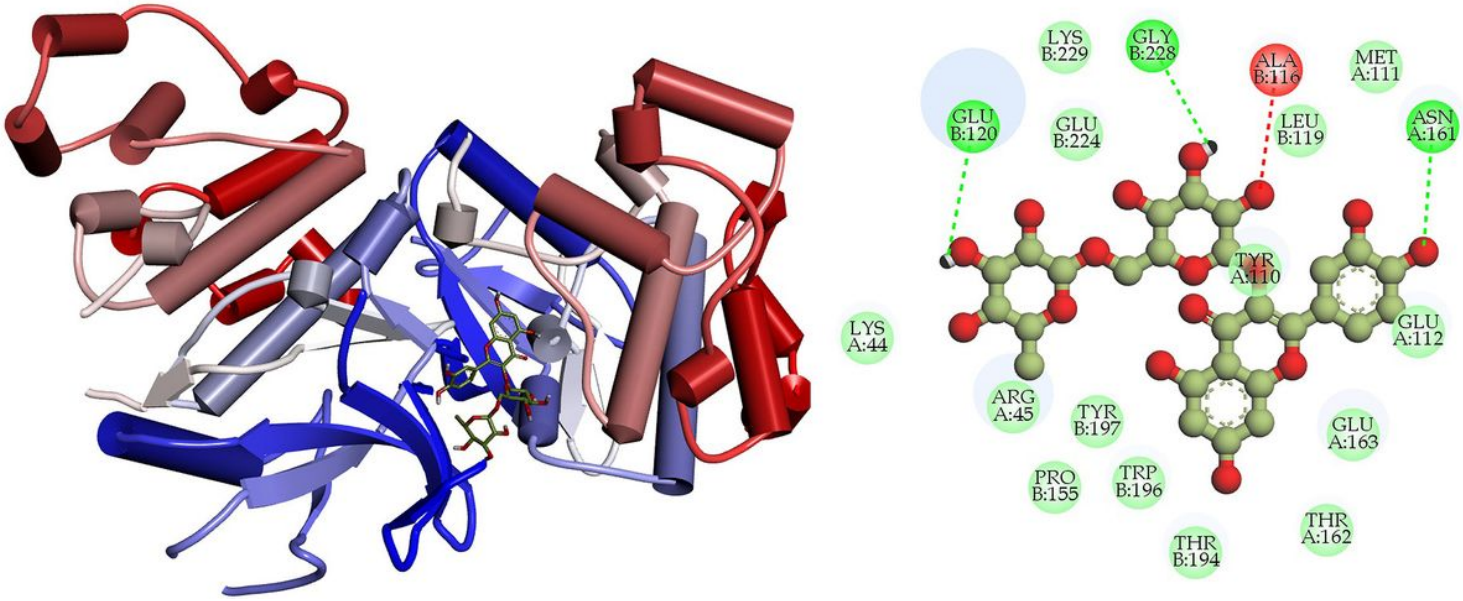


**Figure 6**

Depicted the interaction between the compound CID: 5280805 (Rutin) and MAPK. Left side representing 3D and the right side representing 2D complex protein–ligand interaction.

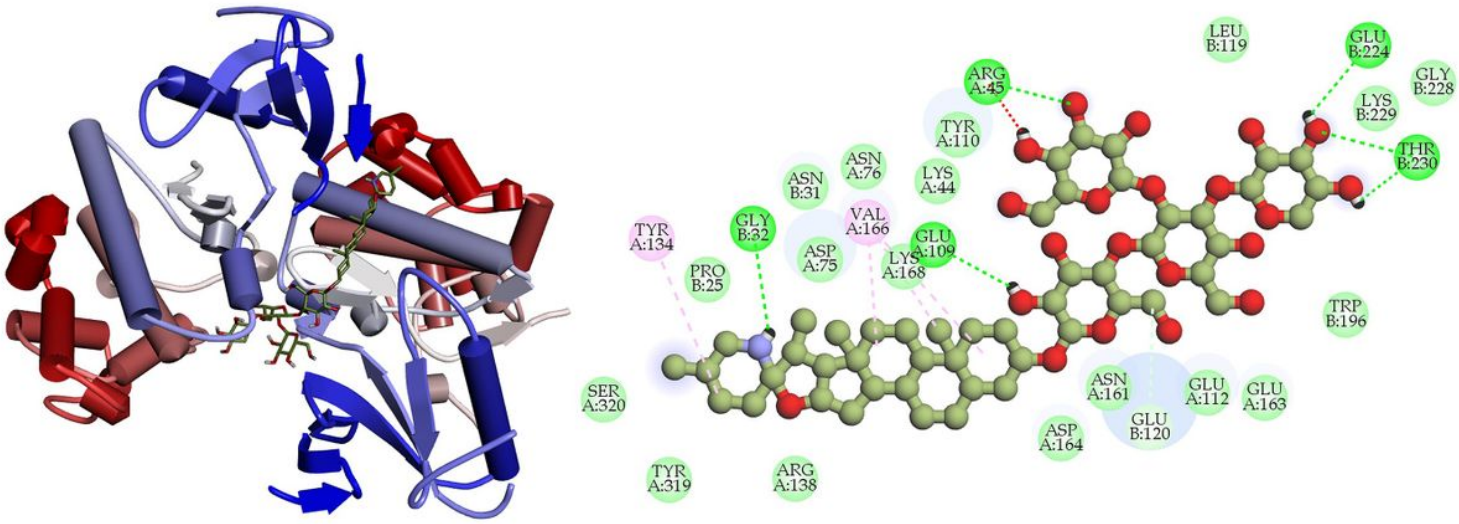


**Figure 7**

Depicted the interaction between the compound CID: 28523 (Tomatine) and MAPK. Left side representing 3D and the right side representing 2D complex protein–ligand interaction.

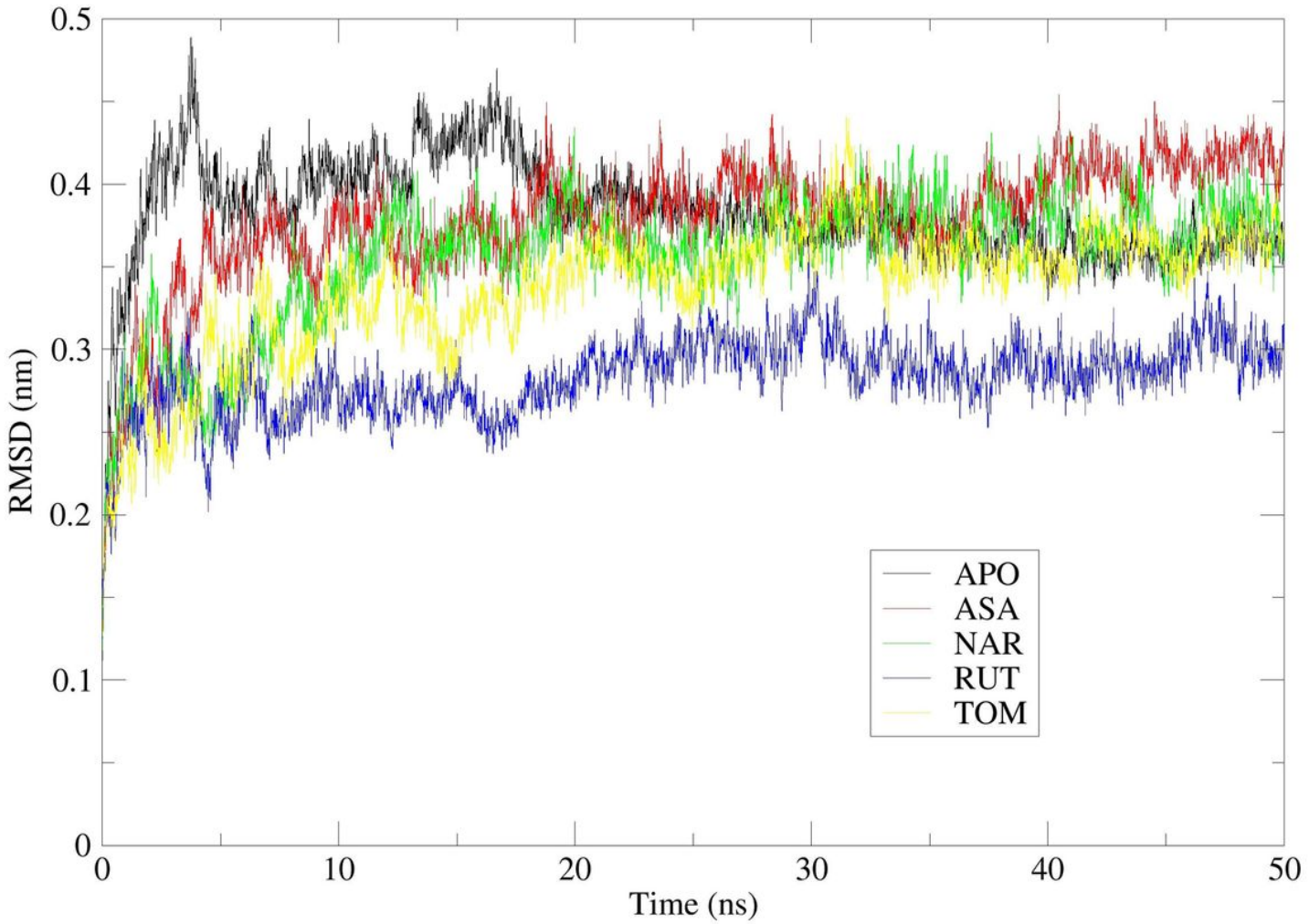


**Figure 8**

RMSD study plot for 50 ns MD Simulation of 7AQB-APO (Black), 7AQB-ASA (Red), 7AQB-NAR (Green), 7AQB-RUT (Blue) and 7AQB-TOM (Yellow).

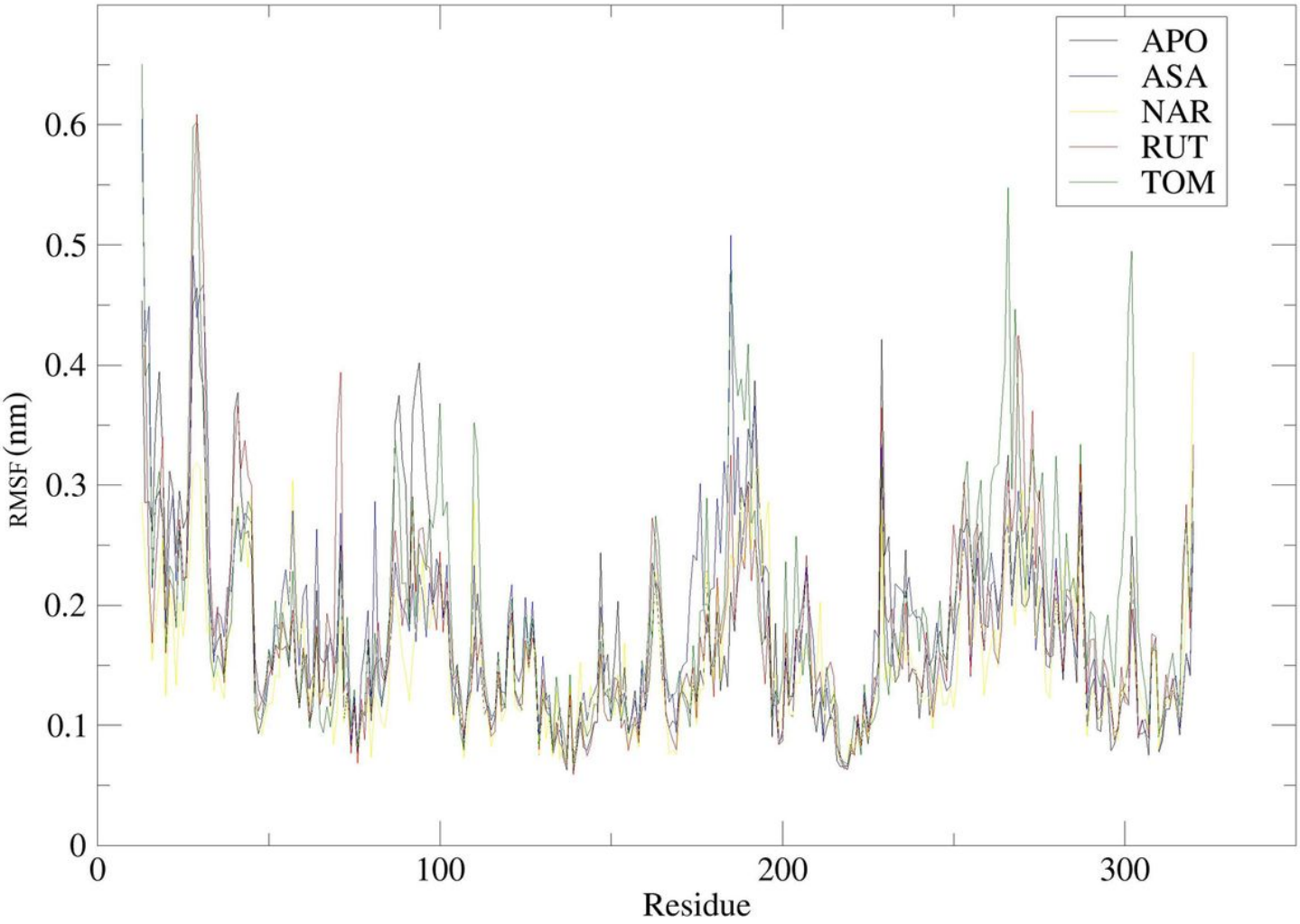


**Figure 9**

RMSF study plots for 50 ns MD Simulation. Chain of 7AQB-APO (Black), 7AQB-ASA (Red), 7AQB-NAR (Green), 7AQB-RUT (Blue) and 7AQB-TOM (Yellow).

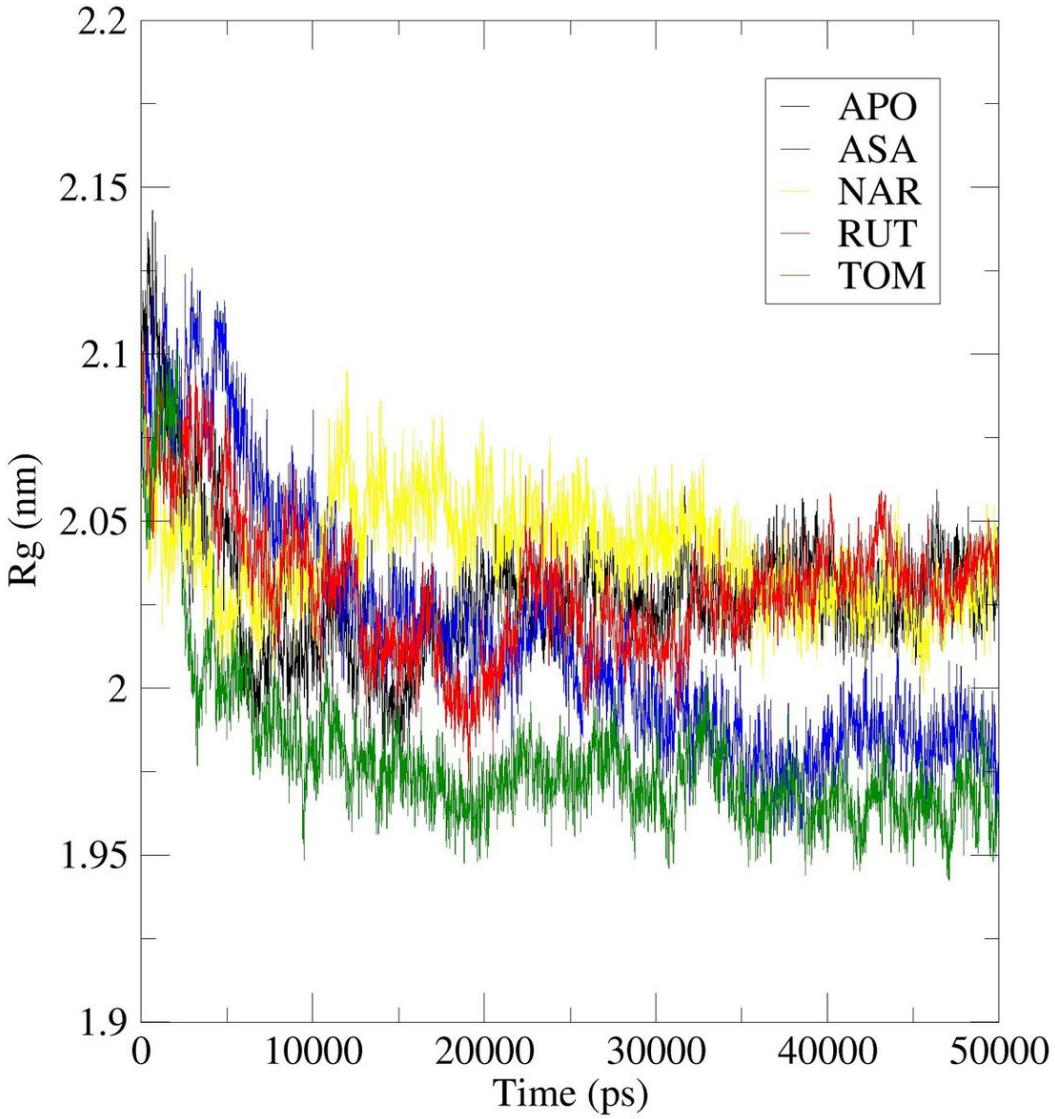


**Figure 10**

Radius of gyration study plot for 50 ns MD Simulation of 7AQB-APO (Black), 7AQB-ASA (Red), 7AQB-NAR (Green), 7AQB-RUT (Blue) and 7AQB-TOM (Yellow).

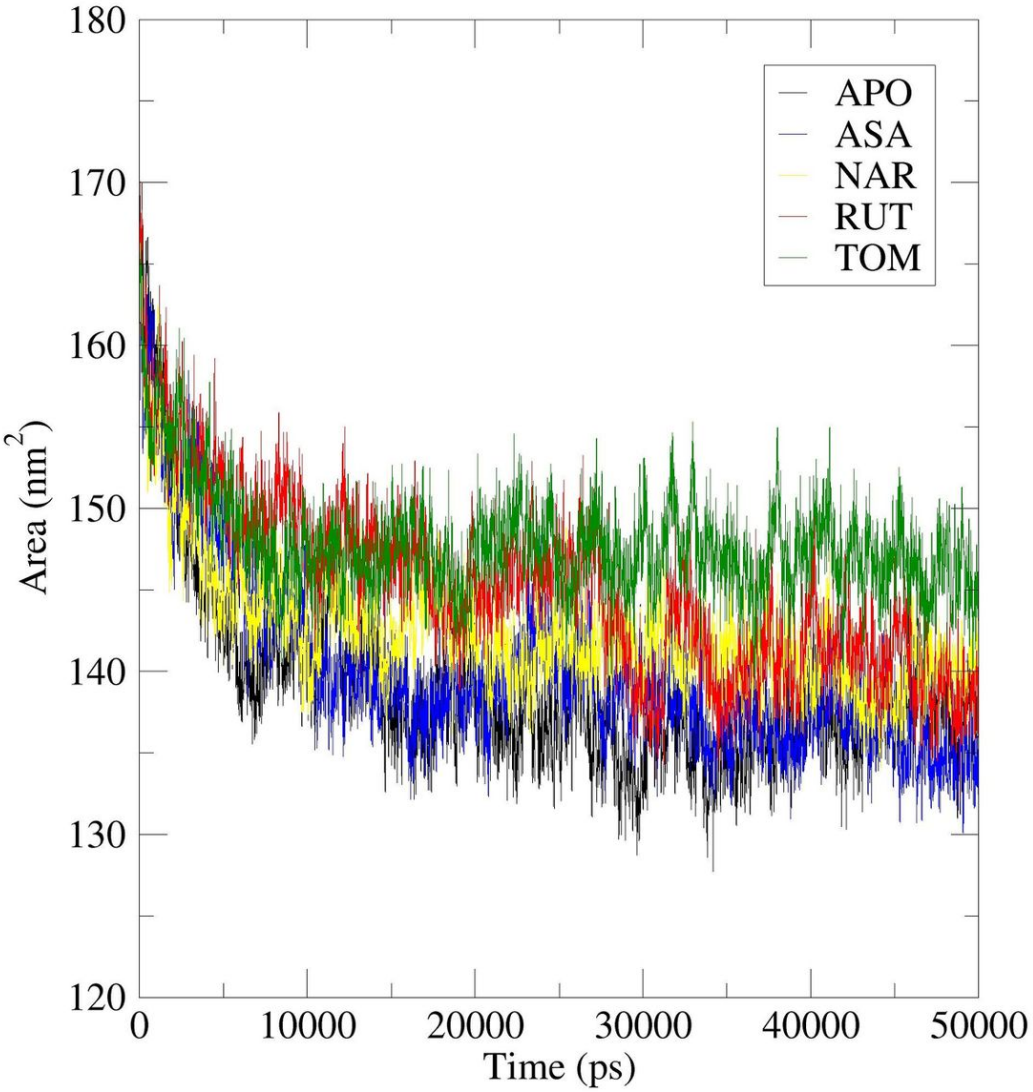


**Figure 11**

Solvent accessible surface area study plot for 50 ns MD Simulation of 7AQB-APO (Black), 7AQB-ASA (Red), 7AQB-NAR (Green), 7AQB-RUT (Blue) and 7AQB-TOM (Yellow).

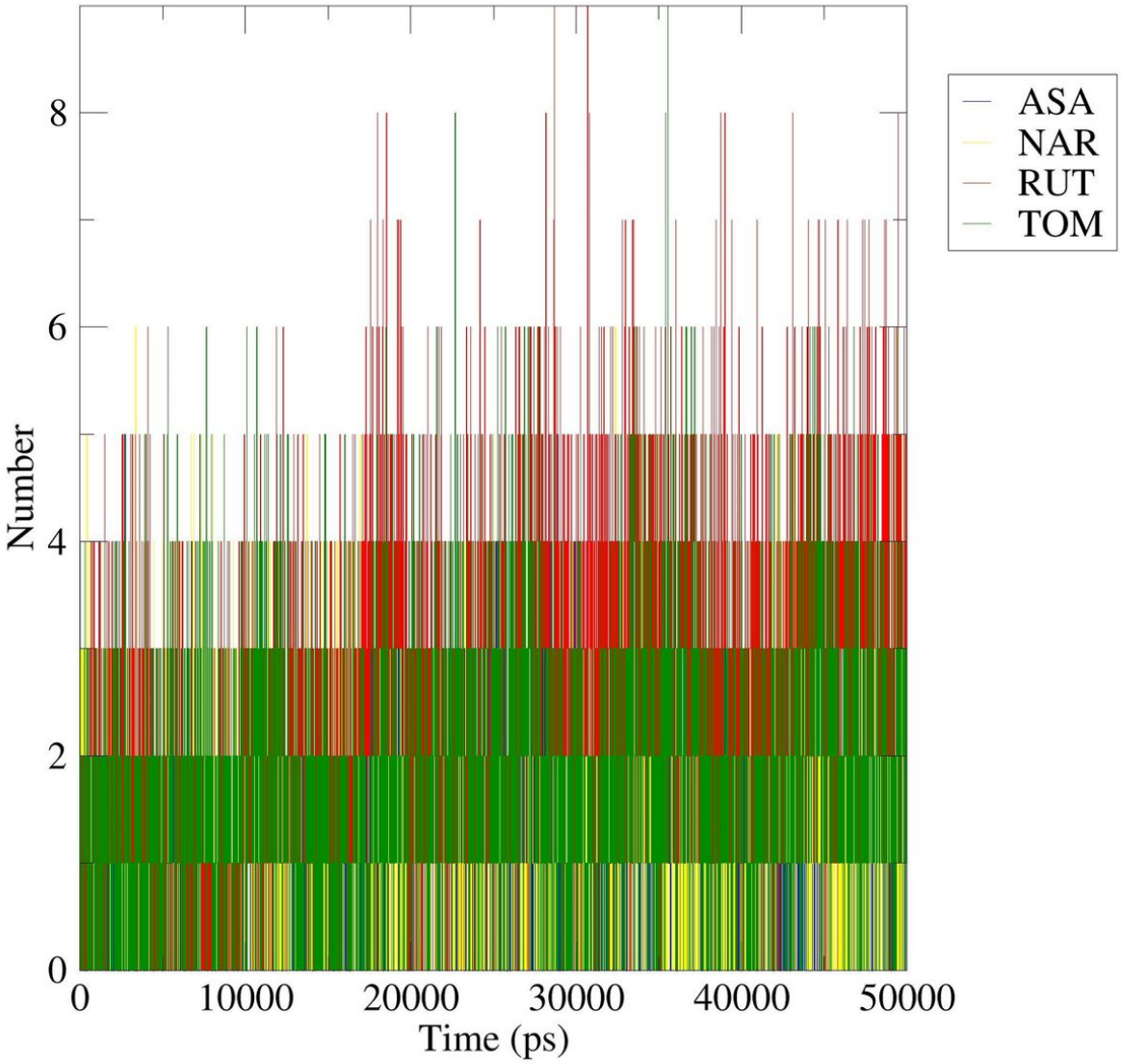


**Figure 12**

Intermolecular hydrogen bonding study plot for 50 ns MD Simulation of 7AQB-APO (Black), 7AQB-ASA (Red), 7AQB-NAR (Green), 7AQB-RUT (Blue) and 7AQB-TOM (Yellow).

## Supplementary Files

This is a list of supplementary files associated with this preprint. Click to download.

- Graphicalabstract.jpg